Numerical investigation of olfactory performance in upwind surging hawkmoth flight

Seth Lionetti¹, Tyson Hedrick², and Chengyu Li³

^{1,3}Department of Mechanical Engineering, Villanova University, Villanova, PA 19085

Flying insects possess sophisticated olfactory systems that they use to find food, locate mates, and avoid predators. It is suspected that insects flap their wings to draw odor plumes toward their antennae. This behavior enhances their olfactory sensitivity and is analogous to sniffing in mammals. However, insects' wing kinematics change drastically as their flight speed increases, and it is unknown how these changes affect the insect's odorant perception. To address this question, we simulated odor-tracking hawkmoth fight at 2 m/s and 4 m/s using an in-house immersed-boundary-method-based CFD solver. The solver was used to solve the Navier-Stokes equations that govern the flow, as well as the advection-diffusion equation that governs the odor transport process. Results show that hawkmoths use their wings to significantly increase the odor intensity along their antennae. However, peak odor intensity is 39% higher during 2 m/s flight than 4 m/s flight. We therefore suspect that insects have greater olfactory performance at lower forward flight speed. Findings from this study could provide inspiration for bio-inspired odor-guided navigation technology.

Nomenclature

ϕ	= Wing stroke angle	t/T	= Normalized time
Ψ	= Wing deviation angle	P^*	= Normalized pressure coefficient
θ	= Wing pitch angle	\overline{U}_{tip}	= Cycle-averaged wing tip velocity
Φ	= Stroke amplitude	f	= Flapping frequency
Re	= Reynolds number	k	= Reduced frequency
C'	= Normalized odor intensity	R	= Wing root-to-tip length
D	= Odor diffusivity	U_{∞}	= Incoming flow speed

1

²Department of Biology, University of North Carolina at Chapel Hill, Chapel Hill, NC 27599, USA

¹PhD student, slionet1@villanova.edu, AIAA Member

² Professor, thedrick@bio.unc.edu, AIAA Member

³ Assistant professor, chengyu.li@villanova.edu, AIAA Member

I. Introduction

THE development of odor-guided navigation technology could lead to transformative advancements in modern unmanned aerial vehicles. Inspiration for this technology can be found in nature. Flying insects possess an advanced olfactory system that they use to detect mates, find food, and avoid predators. During flapping flight, their wings inevitably perturb the odor plumes emitted by these sources. Previous studies on insect olfaction have demonstrated that insects potentially use their wings to draw odor plumes toward their olfactory organs (antennae), a behavior comparable to sniffing in mammals [1, 2]. Insect wings therefore serve a twofold purpose: to generate the aerodynamic forces required for flight, while also increasing the odor concentration around the antennae. As insects seek an odor source, they exhibit two primary flight patterns: crosswind tracking and upwind surging. In crosswind tracking flight, they zigzag side-to-side until they detect a desirable odor, and then they surge upwind toward its source [3, 4]. Previous studies have suggested that insects' olfactory sensitivity during upwind surging flight is highly dependent on their flapping wing kinematics [5].

However, over the past few decades, studies in understanding insect flight have primarily focused on the aerodynamic function of flapping wings, without considering how the wing-induced flow perturbation impacts the airborne odor stimuli. For example, as a hawkmoth's flight speed increases, its wings assume a more horizontal orientation to reduce drag [6]. This shift in wing kinematics reduces the moth's aerodynamic performance, but it remains unknown whether its olfactory performance is similarly affected. In the literature, there have been relatively few studies on how changes in wing kinematics affect insects' olfactory sensitivity. Experimental approaches have been hindered by the small size of insect wings and the inability to non-intrusively measure odor concentration along the antennae. On the other hand, computational fluid dynamics (CFD) approaches can precisely calculate odor concentration anywhere in the fluid domain by solving the advection-diffusion equations. However, previous computational studies on insect olfaction have largely focused on very small insects like fruit flies [5, 7], and there have been no previous studies on how changes in flight speed affect olfactory performance. To address these gaps in knowledge, we aim use numerical simulations to examine how changes in a hawkmoth's flight speed and wing kinematics affect its olfactory performance. Findings from this work will provide inspiration for the design of bio-inspired odor-guided navigation systems.

II. Methodology

A. Experimental setup and flight reconstruction

Hawkmoths engaged in upwind surging odor-tracking flight were recorded while flying at both 2 m/s and 4 m/s. The moths were placed inside a wind tunnel and were allowed to feed from an artificial flower. Recordings were captured using three high-speed cameras operating at 1000 frames per second with a shutter speed of 300 µs. During the experiments, the insects' flight speed was controlled by adjusting the input velocity of the wind tunnel. See our previous study [6] for further details about this experimental setup. We selected recordings of a single individual hawkmoth to be used for 3D model reconstruction and computational simulation.

After recording 2 m/s and 4 m/s upwind surging hawkmoth flight, we created a meshed model hawkmoth using Autodesk Maya. The model hawkmoth was then superimposed over the wind tunnel recordings, and the model wings were adjusted to align with various frames of the high-speed video. Between the selected frames, Fourier interpolation was used to reconstruct one full flapping cycle. Using the reconstructed flight data, we were able to calculate the hawkmoth's wing kinematics for each flight speed. As shown in Figure 1(a), we defined three Euler angles to measure the wing's position relative to

the stroke plane. The wing stroke angle (ψ) gives the location of the wing in the stroke plane and is defined as the angle between the projection of the wing root-to-tip line and the z-axis. The deviation angle (ϕ) provides the angle between the wing root-to-tip line and its projection onto the stroke plane. The wing pitch angle (θ) is defined as the angle between the wing chord and the stroke plane. Figure 1(b) and Figure 1(c) show the time history of the Euler angles for 2 m/s and 4 m/s upwind surging flight, respectively. These plots indicate that the magnitude of the hawkmoth's wing stroke angle increases as its flight speed increases. In addition, the hawkmoth reduces its wing pitch angle as it flies faster.

To measure the hawkmoth's wing tip speed in relation to incoming flow speed, we use the reduced frequency k. This dimensionless parameter is defined by $k = \frac{fR}{U_{\infty}}$, where f is the hawkmoth's flapping frequency, R is the wing root-to-tip length, and U_{∞} is the incoming flow speed. The reduced frequency is equal to 0.76 for 2 m/s flight and 0.41 for 4 m/s flight.

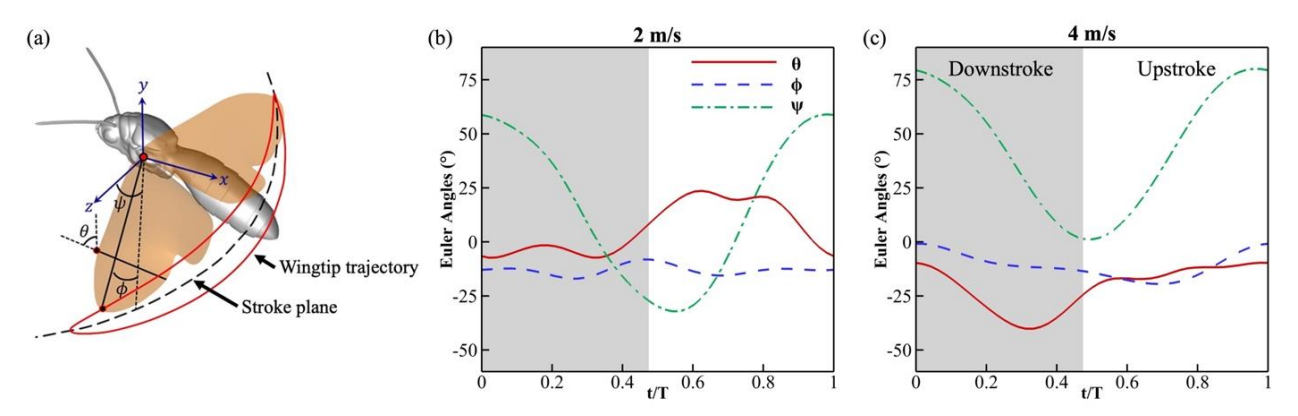


Figure 1. (a) Definition of wing Euler angles. (b) Time history of wing kinematics during 2 m/s upwind surging flight. (c) Time history of wing kinematics during 4 m/s upwind surging flight.

B. Numerical method and simulation setup

We used an in-house immersed-boundary-method-based computational fluid dynamics solver to solve the 3D viscous incompressible Navier-Stokes equations that govern the flow. The nondimensional form of these equations can be written as:

$$\frac{\partial u_i}{\partial x_i} = 0; \quad \frac{\partial u_i}{\partial t} + \frac{\partial (u_i u_j)}{\partial x_i} = -\frac{\partial p}{\partial x_i} + \frac{1}{Re} \frac{\partial}{\partial x_i} \left(\frac{\partial u_i}{\partial x_i} \right) \tag{1}$$

where u_i are the velocity components, p is the pressure, and Re is the Reynolds number.

The above equations are discretized using a collocated cell-centered arrangement of the primitive variables, u_i and p. The equations are integrated in time using a fractional step method, and a second-order difference scheme is used in space. The complex moving boundaries of the flapping wings are handled using an immersed boundary method approach, wherein boundary conditions are imposed via a "ghost-cell" procedure [8]. This approach eliminates the need for complicated remeshing algorithms and greatly reduces the computational cost of simulations. The immersed boundary method employed in the current study has successfully been used to simulate insect flight [5, 7, 9] and odor-tracking behavior [10-12], as well as other

forms of bio-inspired propulsion [9, 13-18]. Validations of the in-house CFD solver employed in this study can be found in our previous papers [6, 19-23].

Odorant transport in the flow field is governed by the advection-diffusion equation, which can be written as:

$$\frac{\partial C'}{\partial t} + u_i \frac{\partial C'}{\partial x_i} = D \frac{\partial^2 C'}{\partial x_i \partial x_i} \tag{2}$$

where u_i are the velocity components; $C' = C/C_0$ is the normalized odor intensity and C_0 is the odor intensity at the odor source; and D is the odor diffusivity. In addition, we define the normalized pressure as $P^* = \frac{2(p-p_\infty)}{\rho \overline{U}_{tip}^2}$. Here, \overline{U}_{tip} is the cycle-averaged wing tip velocity and can be expressed as $2\Phi fR$, in which Φ is the stroke amplitude (91.09° for 2 m/s flight and 81.21° for 4 m/s flight), f is the flapping frequency (27.8 Hz for 2 m/s flight and 30.2 Hz for 4 m/s flight), and R is the wing root-to-tip length (55 mm for all simulation cases).

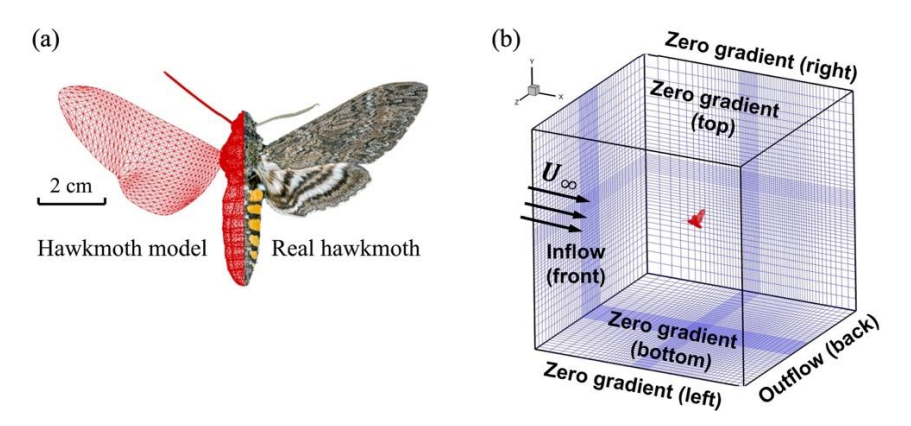


Figure 2. (a) Comparison between the model hawkmoth and a real hawkmoth. (b) Schematic of the computational domain used for simulations.

Figure 2(b) shows a schematic of the computational domain employed in this study. The meshed hawkmoth model was situated within a Cartesian computational grid that contained two defined layers. The hawkmoth model was placed inside a high-density region, which was surrounded by a secondary dense layer. Beyond this layer, the grid was stretched rapidly. An inflow boundary condition was specified at the front of the fluid domain, corresponding to the flight speed of the hawkmoth. Outflow was allowed through the back of the domain, and a zero-gradient boundary condition was applied at all other boundaries. To simulate the odor transport process, a rectangular odor source was placed approximately two body lengths in front of the hawkmoth. All simulations were run for six flapping cycles in order to reach a state of periodic flow. All results reported in this paper are based on the sixth cycle.

III. Results and Discussion

In this section, we present the hawkmoth's aerodynamic and olfactory performance during upwind surging flight at 2 m/s and 4 m/s.

A. Aerodynamic Performance

Figure 3 shows the time history of the hawkmoth's aerodynamic force production during 2 m/s and 4 m/s upwind surging flight. These plots demonstrate that the hawkmoth significantly reduces its drag generation as its flight speed increases. In our previous study [6], we found that the hawkmoth must minimize drag at high forward flight speeds to prevent itself from blowing away in the incoming flow. To achieve this, the hawkmoth reduces its wing pitch angle during the upstroke, as shown in Figure 1(b,c)). However, this shift in wing kinematics also causes the hawkmoth to generate a large amount of negative lift during the upstroke, which limits the total amount of lift it can generate during the flapping cycle. This constraint on lift production explains why hawkmoths are unable to sustain steady forward flight at speeds greater than 4 m/s.

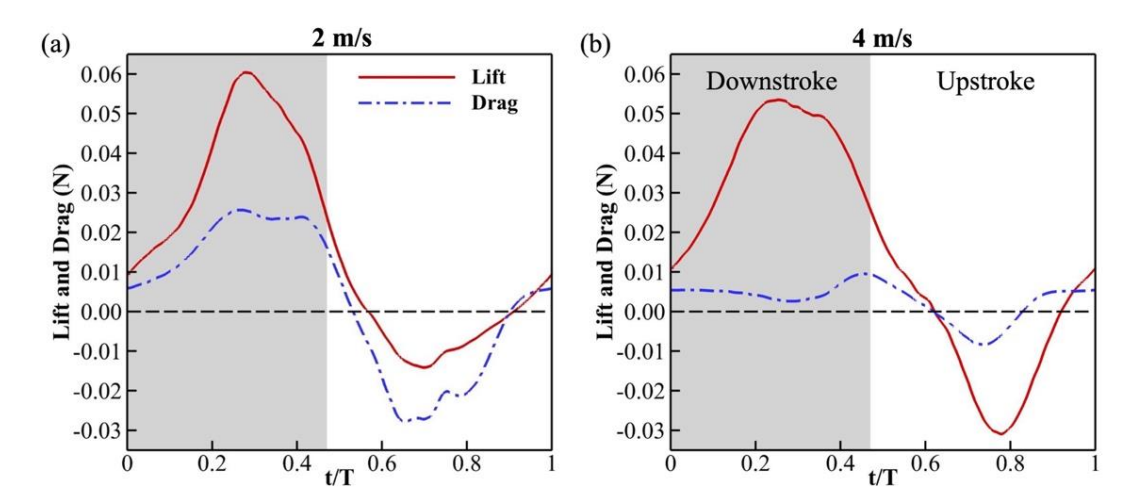


Figure 3. Time history of lift and drag generation during (a) 2 m/s and (b) 4 m/s upwind surging odor-tracking flight.

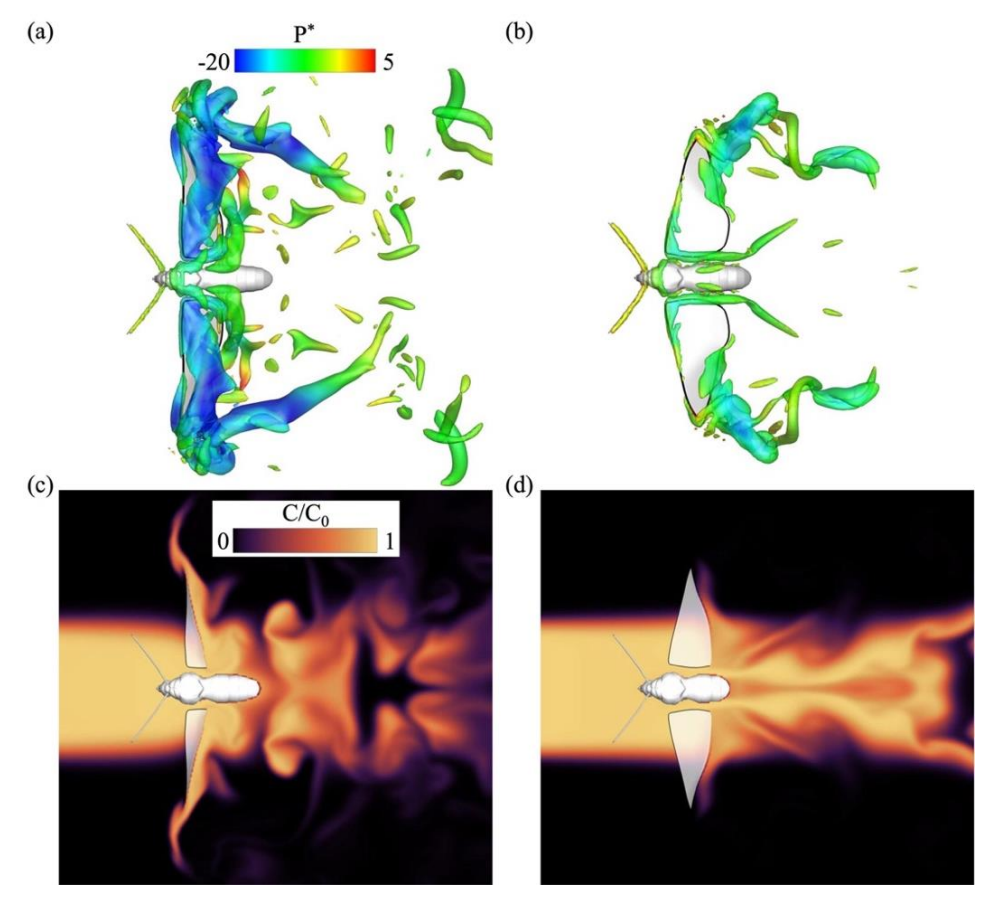


Figure 4. Q-criterion vortex structures at t/T = 0.58 for (a) 2 m/s and (b) 4 m/s upwind surging flight. Vortex structures are colored according to pressure. The odor plume structures at t/T = 0.58 are also shown for (c) 2 m/s and (d) 4m/s upwind surging flight.

B. Olfactory Performance

As the hawkmoth's flight speed increases, it modifies its wing kinematics by reducing its wing pitch angle during the upstroke. In this section, we examine how this shift in wing kinematics affects the wing-induced flow around the hawkmoth's antennae and its related olfactory performance. Figure 4 shows the Q-criterion wake structures and odor plume perturbations produced by the hawkmoth's flapping wings approximately halfway through the downstroke (t/T = 0.58). The Q-criterion wake structures are colored according to the normalized pressure coefficient. During 2 m/s flight, the hawkmoth's wings generate more wake and have a greater effect on the odor plume structures. One reason for this difference is the hawkmoth's wing kinematics during 2 m/s flight. During low-speed flight, the greater wing pitch angle (visible in Figure 4(c)) increases the cross-sectional wing area exposed to the incoming flow. As a result, the flapping wing motion pushes more odor toward the hawkmoth's antennae. Another reason why wing-induced flow is greater during 2 m/s flight (k = 0.71) compared to 4 m/s flight (k = 0.41). This indicates that wing-induced flow is more dominant at lower flight speeds.

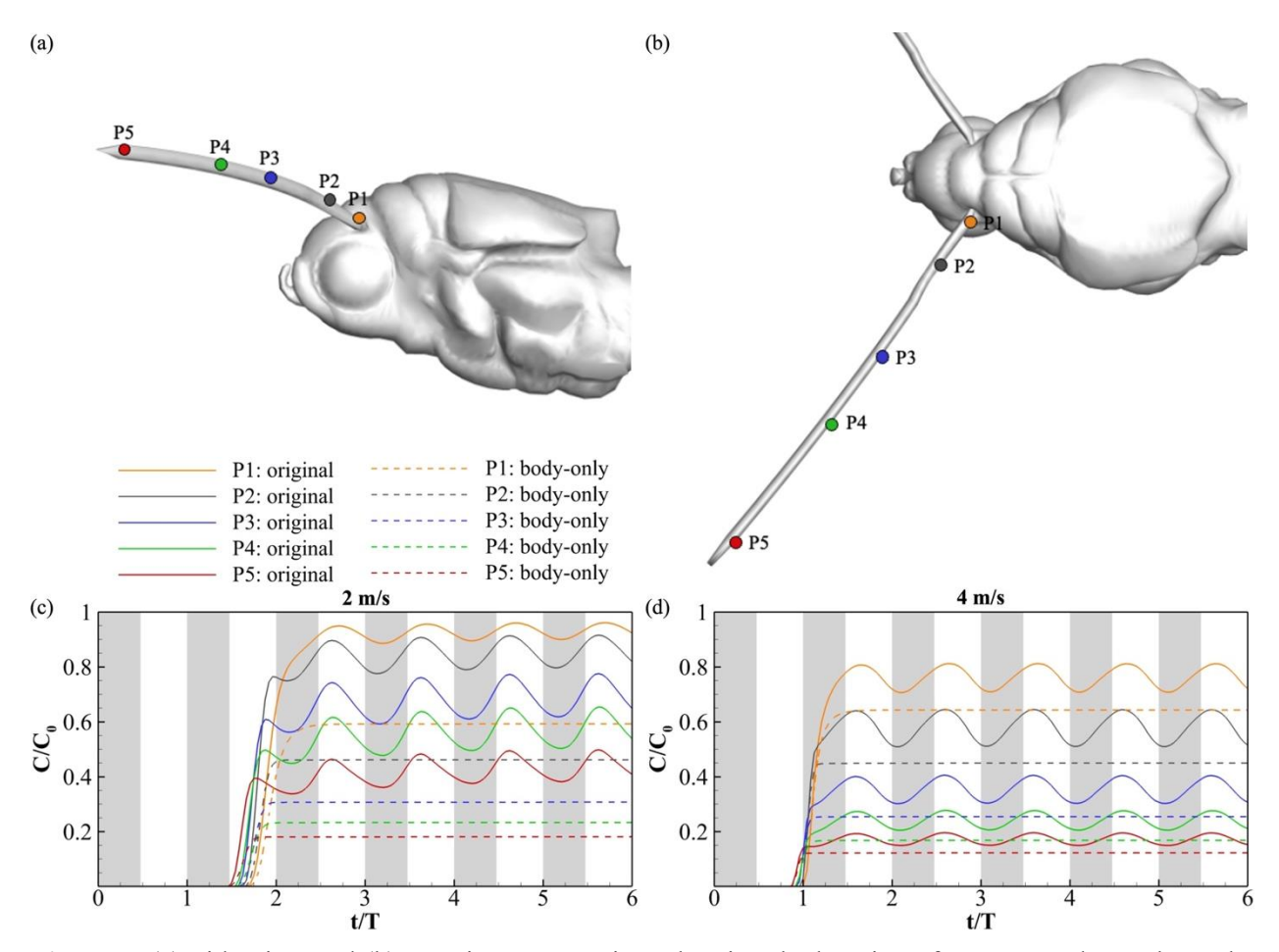


Figure 5. (a) Side-view and (b) top-view perspectives showing the location of antennae odor probes. The odor intensity at each probe is shown for (c) 2 m/s and (d) 4 m/s upwind surging flight.

To more closely examine how flight speed affects the hawkmoth's olfactory performance, we measured the odor intensity at five probe locations along the hawkmoth's antennae, as shown in Figure 5. In this figure, results are also included for body-only simulation cases, which were run without the hawkmoth's flapping wings. For the body-only cases, the odor intensity is steady and is greatest near the base of the antennae. In addition, there is not a significant difference in intensity between the 2 m/s and 4 m/s body-only cases. When the flapping wings are added, the odor intensity significantly increases and begins to fluctuate. For both flight speeds, the odor intensity peaks near the beginning of the upstroke. The increase in odor intensity caused by the flapping wings is much greater during 2 m/s upwind surging flight. This is a result of the greater wing-induced flow and larger reduced frequency observed at lower flight speeds. Based on these results, we can conclude that lower flight speeds are better suited for odor-tracking flight in hawkmoths.

Acknowledgments

This work was supported by the National Science Foundation to C. Li (NSF CBET-2042368) and to T. L. Hedrick (NSF IIS-1239212). All simulations were run on the High-Performance Computing Cluster of the College of Engineering at Villanova University.

References

- [1] C. Loudon and M. Koehl, "Sniffing by a silkworm moth: wing fanning enhances air penetration through and pheromone interception by antennae," *Journal of experimental Biology*, vol. 203, no. 19, pp. 2977-2990, 2000.
- [2] S. P. Sane and N. P. Jacobson, "Induced airflow in flying insects II. Measurement of induced flow," *Journal of Experimental Biology*, vol. 209, no. 1, pp. 43-56, 2006.
- [3] L. L. López *et al.*, "Moth-like chemo-source localization and classification on an indoor autonomous robot," in *On Biomimetics*: IntechOpen, 2011.
- [4] K. A. Justus, S. W. Schofield, J. Murlis, and R. T. Cardé, "Flight behaviour of Cadra cautella males in rapidly pulsed pheromone plumes," *Physiological Entomology*, vol. 27, no. 1, pp. 58-66, 2002.
- [5] C. Li, H. Dong, and K. Zhao, "A balance between aerodynamic and olfactory performance during flight in Drosophila," *Nature Communications*, vol. 9, no. 1, pp. 1-8, 2018.
- [6] S. Lionetti, T. L. Hedrick, and C. Li, "Aerodynamic explanation of flight speed limits in hawkmoth-like flapping-wing insects," *Physical Review Fluids*, vol. 7, no. 9, p. 093104, 2022.
- [7] C. Li, "Effects of wing pitch kinematics on both aerodynamic and olfactory functions in an upwind surge," *Proceedings of the Institution of Mechanical Engineers, Part C: Journal of Mechanical Engineering Science*, vol. 235, no. 2, pp. 296-307, 2021.
- [8] R. Mittal, H. Dong, M. Bozkurttas, F. Najjar, A. Vargas, and A. Von Loebbecke, "A versatile sharp interface immersed boundary method for incompressible flows with complex boundaries," *Journal of computational physics*, vol. 227, no. 10, pp. 4825-4852, 2008.
- [9] C. Li, H. Dong, and K. Zhao, "Dual functions of insect wings in an odor-guided aeronautic navigation," *Journal of Fluids Engineering*, vol. 142, no. 3, p. 030902, 2020.
- [10] M. Lei and C. Li, "A Balance Between Odor Intensity and Odor Perception Range in Odor-Guided Flapping Flight," in *ASME 2022 Fluids Engineering Division Summer Meeting*, 2022, vol. Volume 2: Multiphase Flow (MFTC); Computational Fluid Dynamics (CFDTC); Micro and Nano Fluid Dynamics (MNFDTC), V002T05A002, ASME FEDSM 2022-85407.
- [11] M. Lei and C. Li, "Effects of Wing Kinematics on Modulating Odor Plume Structures in the Odor Tracking Flight of Fruit Flies," in *ASME 2021 Fluids Engineering Division Summer Meeting*, 2021, vol. Volume 1: Aerospace Engineering Division Joint Track; Computational Fluid Dynamics, V001T02A022, ASME FEDSM 2021-61832.
- [12] M. Lei and C. Li, "Numerical investigation of the passive pitching mechanism in odor-tracking flights," in *AIAA AVIATION 2020 FORUM*, AIAA 2020-3016.

- [13] C. Li, H. Dong, and B. Cheng, "Tip vortices formation and evolution of rotating wings at low Reynolds numbers," *Physics of Fluids*, vol. 32, no. 2, p. 021905, 2020.
- [14] C. Li, J. Wang, G. Liu, X. Deng, and H. Dong, "Passive Pitching Mechanism of Three-Dimensional Flapping Wings in Hovering Flight," San Francisco, CA, USA (ASME 2019) V002T02A043, in Proceedings of the 8th Joint Fluids Engineering Conference on ASME-JSME-KSME 2019, AJKFluids 2019-4639, 2019.
- [15] M. Lei, J. P. Crimaldi, and C. Li, "Navigation in odor plumes: How do the flapping kinematics modulate the odor landscape?," *AIAA paper*, 2021-2817, 2021.
- [16] M. Xu, M. Wei, C. Li, and H. Dong, "Adjoint-based optimization for thrust performance of three-dimensional pitching-rolling plate," *AIAA Journal*, vol. 57, no. 9, pp. 3716-3727, 2019.
- [17] A. Menzer, C. Li, F. Fish, Y. Gong, and H. Dong, "Modeling and Computation of Batoid Swimming Inspired Pitching Impact on Wake Structure and Hydrodynamic Performance," in *ASME 2022 Fluids Engineering Division Summer Meeting*, 2022, vol. Volume 2: Multiphase Flow (MFTC); Computational Fluid Dynamics (CFDTC); Micro and Nano Fluid Dynamics (MNFDTC), V002T05A003, ASME FEDSM 2022-86684.
- [18] Z. Lou, A. Herrera-Amaya, M. L. Byron, and C. Li, "Hydrodynamics of Metachronal Motion: Effects of Spatial Asymmetry on the Flow Interaction Between Adjacent Appendages," in *ASME 2022 Fluids Engineering Division Summer Meeting*, 2022, vol. Volume 2: Multiphase Flow (MFTC); Computational Fluid Dynamics (CFDTC); Micro and Nano Fluid Dynamics (MNFDTC), V002T05A016, ASME FEDSM 2022-86967.
- [19] C. Li, H. Dong, and G. Liu, "Effects of a dynamic trailing-edge flap on the aerodynamic performance and flow structures in hovering flight," *Journal of Fluids and Structures*, vol. 58, pp. 49-65, 2015.
- [20] C. Li and H. Dong, "Wing kinematics measurement and aerodynamics of a dragonfly in turning flight," *Bioinspiration & biomimetics*, vol. 12, no. 2, p. 026001, 2017.
- [21] C. Li, J. Jiang, H. Dong, and K. Zhao, "Computational modeling and validation of human nasal airflow under various breathing conditions," *Journal of Biomechanics*, vol. 64, no. 7, pp. 59-68, 2017.
- [22] M. Lei and C. Li, "The aerodynamic performance of passive wing pitch in hovering flight," *Physics of Fluids*, vol. 32, no. 5, p. 051902, 2020.
- [23] Y. Liu, A. D. Lozano, T. L. Hedrick, and C. Li, "Comparison of experimental and numerical studies on the flow structures of hovering hawkmoths," *Journal of Fluids and Structures*, vol. 107, p. 103405, 2021.